IEICE TRANS. ELECTRON., VOL.E101–C, NO.7 JULY 2018

INVITED PAPER *Special Section on Distinguished Papers in Photonics*

A Lens-Integrated Surface-Emitting DFB Laser and Its Application to Cost-Effective Single-Mode Optical Sub Assembly*

Koichiro ADACHI[†a)], **Takanori SUZUKI**[†], ***and*** **Shigehisa TANAKA**[†], ***Members***

SUMMARY A lens-integrated surface-emitting DFB laser and its application to low-cost single-mode optical sub-assemblies (OSAs) are discussed. By using the LISEL, high-efficient optical coupling with reduced number of optical components and non-hermetic packaging are demonstrated. Designing the integrated lens of LISELs makes it possible to achieve passive alignment optical coupling to an SMF without the need for an additional lens. For SiP coupling, the light-emission angle from the LISEL can be controlled by the mirror angle and by displacing the lens. The capability for a low coupling loss of 3.9 dB between the LISEL and a grating coupler on the SiP platform was demonstrated. The LISEL with facet-free structure, integrating DBR mirror, PD, and window structure on its end facet, showed the same lasing performance as the conventional laser with AR facet coating. A storage test (200-hour saturated pressure-cooker test (PCT) at 138°C and 85% RH.) showed that the lasing characteristics did not degrade with high-humidity, demonstrating the potential for applying non-hermetic packaging. Our results indicate that the LISEL is one of the promising light sources for creating cost-effective OSAs.

key words: *surface-emitting laser, integrated optics*

1. Introduction

Data traffic in networks is growing explosively because of the rapid growth of cloud computing and mobile devices all over the world. Especially, the data-transmission capacity of interconnections in data centers (DCs) needs to be increased to handle these large amounts of data traffic. Therefore, High-capacity optical transceivers (TRVs) with data rate of 100Gbps now and 200 and 400Gbps in future are required. DCs have many connections (or "links") between switches (e.g., top of rack (TOR), leaf, spine, and core switches). Since main link distances between these switches in recent mega DCs is up to 2 km, single-mode fibers (SMFs) are need to be utilized instead of conventional multi-mode fibers (MMFs). High-capacity optical TRVs using SMFs with data rates of beyond 100Gbps are therefore required to offer these networks.

In general, there are three approaches in order to increase the data rate of TRVs. The first is multi-level modulation such as n-level pulse amplitude modulation (PAM-n). The modulation format in the 400GbE standardization is based on PAM4 [1]. The second is wavelength division multiplexing (WDM), and 100G-CWDM4 multi-source agreement (MSA) whose link distance is up to 2 km was established for interconnections in DCs [2]. In this MSA, 4-wavelength optical signals of 25Gbps are optically multiplexed and de-multiplexed in TRVs to increase the bit rate in one SMF. The third is spatial division multiplexing (SDM). In this approach, optical transmission using a multi core fiber or parallel-array fibers increases the data capacity. 100G parallel single-mode 4-lane (PSM4)-MSA, whose link distance is up to 500 m, was established for interconnects in DCs [3]. 100G-PSM4 is based on a 25-Gbps × 4-lane parallel SMF.

In the DC, a cost effective network is strongly required in addition to increasing the capacity. Since the network cost is a summation of the optical fiber cost and TRV cost, the cost-effective TRVs are strongly required. Reducing the cost of the optical sub-assembly (OSA) enables cost-effective TRVs to be created efficiently because the OSA cost dominates most of their cost. Reducing the number of components and simplifying their assembly process are general approaches to producing cost-effective OSAs. In terms of required number of SMFs, TRVs with PSM4 (in generally, PSM-n) need more cost-effective configuration in the OSA as compared to that with WDM.

In the case of the PSM4, two candidates have been proposed for the OSA; one is a 1.3-μm direct-modulation laser (DML) with uncooled operation [4], and the other is a silicon photonics (SiP) transmitter [5], [6]. Because the former uses a conventional DML array based on mature InP technologies, it can be expected to be highly reliable as a light source. However, the optical coupling between the DML array and SMF array is complicated and costly because additional optical components, such as optical lens arrays, are required. Simple optical-coupling technology based on a reduced number of optical components is consequently needed to achieve cost-effective OSAs. The latter OSA based on a SiP platform utilizing CMOS technology enables the manufacturing, testing, and packaging costs of the OSAs to be reduced. Hybrid integration of an InP-based DFB laser through a grating coupler (GC) on the SiP platform has been reported as a promising approach to introducing a reliable light source [7]. However, the disadvantages of the hybrid-integration approach are a large footprint and a large number of components (e.g., a lens, a mirror, and an isolator). One of the key issues concerning these OSAs is, therefore, highly efficient optical coupling from the light source with reducing optical components. A precise and complex alignment process can also be a cause of cost increase.

Manuscript received November 6, 2017.
Manuscript revised February 14, 2018.
*This is a review article.
†The authors are with Oclaro Japan, Inc., Sagamihara-shi, 252–5250 Japan.
a) E-mail: koichiro.adachi@oclaro.com
DOI: 10.1587/transele.E101.C.566

Optical-coupling technologies that realize a high coupling efficiency in cost-effective ways are still being developed. For example, microelectrical mechanical system (MEMS) technology has been utilized for the alignment process [8]. Another technology using a high-power laser for aligning the lens position precisely has been proposed [9]. These optical alignment technologies can attain a high optical-coupling efficiency between lasers and the planar light-wave circuit (PLC) or fibers. They, however, require particular components as well as additional processes. It is ideal to obtain optical coupling by passive alignment with no additional components and processes.

Another key issue in regard to achieving a cost-effective OSA is a non-hermetic packaging. Current OSAs using InP-based DFBs generally use expensive hermetic packages (i.e., so-called gold boxes) [10]. This is because a DFB laser needs cleaved facets and facet coatings, and facet coatings sometimes cause degradation of lasing performance, particularly in high-humid conditions [11]. Therefore, a laser that can operate under high-humid condition is in high demand [12].

In order to meet these requirements, we proposed a lens-integrated surface-emitting DFB laser (LISEL) consisting of a DFB laser, integrated mirror, and integrated lens and developed it for a high-capacity and low-cost optical module [13], [14]. By adopting a short cavity DFB structure, we have demonstrated its high-speed operation up to 40Gbps [15]. We have also achieved high-efficient direct optical coupling of a LISEL to a SMF due to its very narrow far-filed pattern [16].

In this paper, we focus to discuss the LISEL and its application to a low-cost single-mode optical module. The concept of the LISEL and low-cost OSAs using it are precisely explained in Sect. 2. Experimental results of optical coupling characteristics including a passive-alignment technique to a SMF array and the SiP platform are described with suitable LISEL design for each application in Sect. 3. Finally, a LISEL with a facet-free structure for non-hermetic package and measured result of high-humid and high-pressure storage test (200-hours saturated pressure-cooker test (PCT) at 138°C and 85% RH) are presented.

2. Concept and Design

2.1 Lens-Integrated Surface-Emitting DFB Laser

Figure 1 shows a schematic structure of the LISEL, which monolithically integrates a 45° total-reflection mirror and aspheric lens into a DFB laser [13]. Light is emitted from the surface of the LISEL by means of an integrated mirror. The optical-mode field pattern from the LISEL is mainly controlled by the radius of curvature (R) of the integrated lens and the distance between the vertex of the integrated lens and the edge of multi-quantum wells (MQW) (D). Because the integrated lens is fabricated using both dry and wet etching, R is controlled using both the photo mask pattern and etching condition [17]. When D is constant, a divergent beam can be emitted in the case of a large R. In contrast, a focused beam can be emitted in the case of a small R. D is mainly determined using the chip thickness, which is over 100 μm.

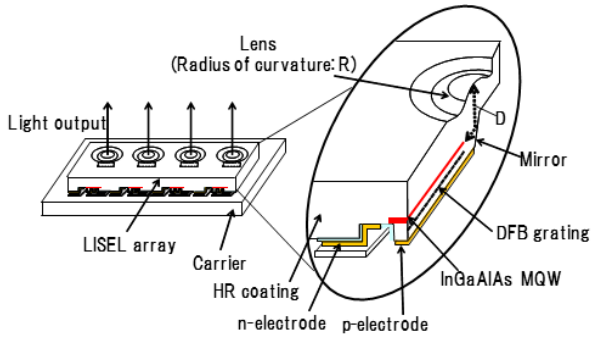

Fig. 1 Schematic structure of 4-ch LISEL array. Enlarge view shows cross section of the DFB laser stripe.

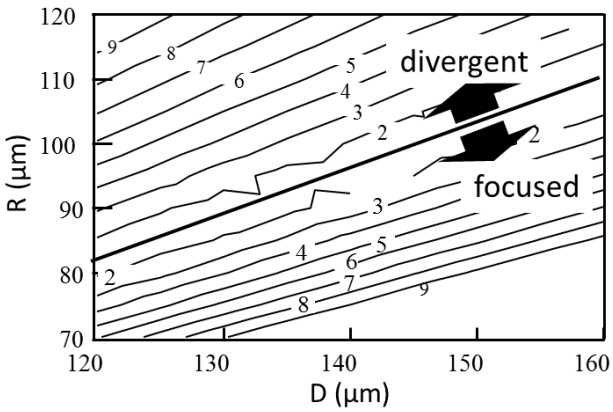

Fig. 2 Contour plots of calculated angle of far-filed pattern form LISEL.

An angle of the far-filed pattern from the LISEL was calculated based on Gaussian optics. Contour plots of the angle as a function of R and D are shown in Fig. 2. The integrated lens of the LISEL was assumed to be spherical. As shown in the contour map, the angle can be determined using R and D from divergent beam to focused beam. Moreover, very narrow far-filed pattern around several degrees is possible as compared to the conventional DFB whose far-filed pattern is around 30°. For example, pairs of R and D that resulted in focused beam with the far-filed pattern around 2° were 90 and 140 μm, respectively.

2.2 Concept of OSA Using LISEL

Conceptual structures of cost-effective OSAs using the LISEL are shown in Fig. 3. Figure 3(a) shows an image of the optical TRV in a quad small form-factor pluggable (QSFP) size. The main optical engine shown in Fig. 3(a) is a LISEL based OSA comprised of a 4-ch LISEL array, 4-ch PD, package, guide pins for a mechanically transferable (MT) connector, and SMF array with the MT connector.

In the case of 100G-PSM4, each channel of the 4-ch LISEL array, which is mounted on a package, is operated at

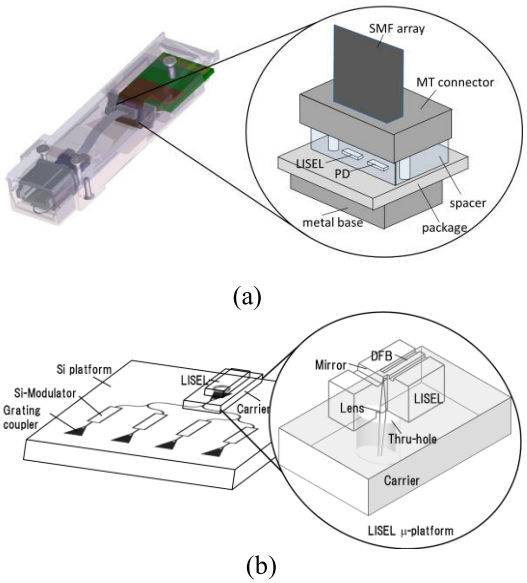

Fig. 3 Conceptual structure of cost-effective OSA with LISEL. (a) Image of optical module and OSA consisting of passively aligned LISEL array and SMF array. (b) OSA consisting of silicon platform integrated with LISEL μ-platform as light source.

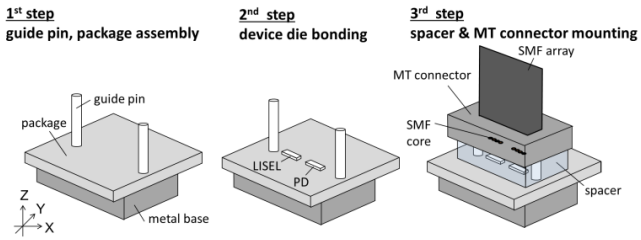

Fig. 4 Assemble process of OSA consists of 4-ch LISEL array and SMF array (MT connector).

25 Gbps. This OSA does not have discrete lenses between the LISEL array and SMF array. Because a MT connector is set near the LISEL, light emitted from each LISEL is directly coupled to the SMF. Therefore, the configuration of the OSA is much simpler in comparison with a conventional one that has an edge-emitting (EE)-DFB laser and additional optical components. The pitch between each LISEL is equal to that between each SMF in the SMF array, normally 250 μm. Thus, the footprint of the OSA is very small.

In Fig. 3(b), an OSA consisting of a LISEL μ-platform (operated as a continuous-wave (CW) laser source) and SiP platform is shown. The LISEL μ-platform consists of only two components: a LISEL and a carrier on which the LISEL is mounted. If the carrier is made of an opaque material for a 1.3-μm laser source, a thru-hole is required in the carrier. On the SiP platform, integrated SiP circuits consisting of external modulators, grating couplers (GCs), and 3-dB couplers are fabricated on a silicon-on-insulator (SOI) substrate.

The light emitted from the LISEL passes through the optical carrier and is directly coupled to the SiP platform via a GC. The spot size of the emitted beam from the LISEL can be adjusted to that of GC by an integrated lens design and distance (thickness of the carrier) between the LISEL and GC. The light coupled to the GC is divided into four paths, which are connected to four modulators by three 3-dB couplers. Light modulated by the four modulators is coupled to the SMF array through the GCs.

3. Optical Coupling

3.1 Passive-Alignment Optical Coupling to SMF

Figure 4 shows the assembly process of the OSA using a 4-ch LISEL array and a SMF array (MT connector). During the assembly, the base position of the package is determined by the guide pins. The position between the guide pins and SMF array is determined by the tolerance specification of the MT connector, which is less than ± 1.4 μm. The relative displacement between the LISEL array and guide pins mainly depends on the alignment accuracy of the bonding of the LISEL die. In this study, we used a commercially-available high-accuracy die bonder with an alignment accuracy of ± 0.5 μm. The LISEL array and SMF array was therefore able to be aligned with a position accuracy of ± 1.5 μm (mean square value). On the other hand, tolerance for the distance between the LISEL array and the SMF array is estimated to be ± 22 μm taking into account thicknesses of spacer, device, and Au bump. To use passive alignment technology for cost-effective OSAs, a position and distance tolerance of less than ± 1.5 μm and $\pm 22\mu$m between the LISEL and SMF is required, respectively. To satisfy this requirement, the LISEL and integrated lens were designed to have a focused beam with R, D, and spot size of emission beam at focused point of 90 μm, 175 μm, and 5.2 μm at $1/e^2$ power width, respectively. In this case excess loss for displacement of $\pm 1.5\mu$m in X and Y direction is only 0.7 dB at the focused point. And excess loss for Z direction in ± 22 μm from the focused point is only 0.4 dB.

Figure 5 shows the measured coupling efficiency between a fabricated LISEL and a SMF with respect to the SMF position at the beam focused point. The peak position of the measured data was slightly shifted from the centre because of the experimental setup. As shown in this graph, the measured coupling efficiency is lower than the design value (R is 90 μm and D is 175 μm). The calculated coupling efficiency, reflecting the fabricated lens shape (i.e., R of 80 μm), is also plotted in Fig. 5 and agreed well with the measurement result. This agreement indicates the degradation of the coupling efficiency can be explained by the deviation of the lens shape (R). The deviation is caused by processing error in this case. (We previously established lens-fabrication process, and confirmed that R can be adjusted by optimizing etching conditions [17].)

Photographs of the fabricated OSA are shown in Fig. 6. An 8°-tilted connector, set just above the LISEL array, is used to mitigate back reflection. To realize both high-coupling efficiency and large displacement tolerance in the in-plane direction, the distance between the LISEL array

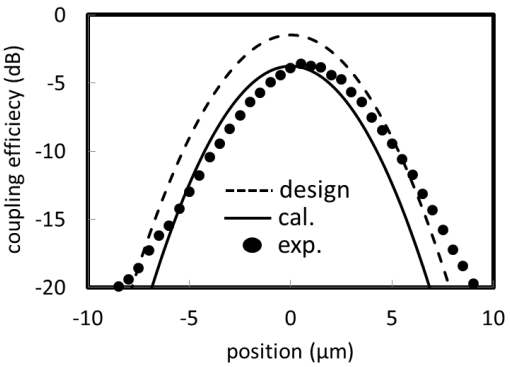

Fig. 5 Measured and calculated coupling efficiency between the LISEL and SMF with respect to the SMF position.

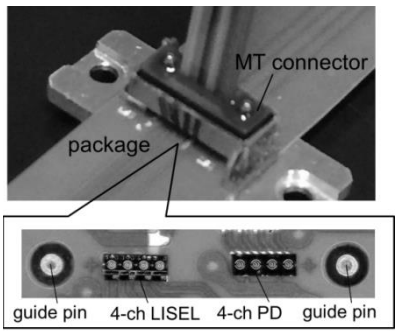

Fig. 6 Photograph of the fabricated OSA. Enlarge shows the 4ch-LISEL array and PD array bonded on the package.

and the MT connector was designed so that beams from the LISEL array are slightly defocused at the connector edge.

The position of the LISEL array was determined by the guide pins, and it was bonded on the package in that position. Then, the MT connector was passively aligned by using the guide pins.

Measured coupling efficiency between the LISEL array and the SMF array in the MT connector is shown in Fig. 7. Calculated deviation of the coupling efficiency (from −3.68 dB to −2.24 dB) for displacement of in-plane direction (+/ − 1.5 μm) and the distance between the LISEL and the MT connector (with the LISEL with R of 90 μm) is also plotted. The 8°-tilted connector was also taken into account in the calculation. The LISEL used in this experiment was designed to have the output power around 6 to 7 dBm at 85°C [13]. So, the OSA was designed to have the minimum output power around 2 dBm at 85°C, which is enough to realize optical module compliant with PSM4 even at high temperature [3].

The measured coupling efficiencies ranged from −6.54 to −5.46 dB, which are lower than the calculated efficiencies. This difference between the measurement and calculation results includes the effects of both the deviation of the R and the relative displacement between the LISEL array and SMF array. To extract the intrinsic feature of the displacement of die bonding, the effect of R was subtracted from these results based on the analysis shown in Fig. 5. The tri-

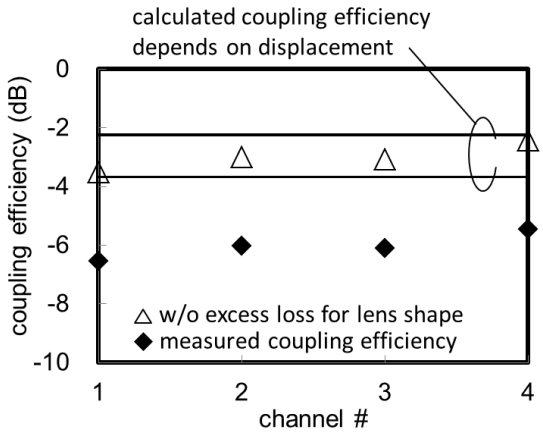

Fig. 7 Coupling efficiency between LISEL array and SMF array by using passive optical alignment technique.

angular points in Fig. 7 show the coupling efficiency only depends on the displacement caused by the passive alignment. As shown in the graph, coupling efficiencies ranged from −3.51 to −2.43 dB, which all channels are within the calculated coupling-efficiency deviation. Moreover, deviation (for 3 sigma) of coupling efficiency within the array is only 1.33 dB. These results indicate that the passive alignment array optical coupling can be expected by using the LISEL array with optimized lens design.

3.2 Optical Coupling to SiP Platform

For optical coupling from the LISEL μ-platform to the SiP platform, the emitted light from the LISEL needs to be optimized to obtain a high coupling efficiency for the GC on the SiP platform. In this optimization, two parameters must be considered: the incident angle of the emitted light from the LISEL to the GC and the spot size of the beam at the surface of the GC. The incident angle to the GC has to be adjusted to the diffraction angle of the GC. In addition, the size of the beam waist from the LISEL should match the size of the GC, and the position of the beam waist should be set at the GC. Therefore, the thickness of the carrier is set in consideration of the lens design of the LISEL.

Figure 8 explains the principle of the emission-angle control of the LISEL. Figure 8(a) shows the standard configuration for vertical emission. By shifting the position of the lens, the emission beam can be angled as shown in Fig. 8(b). In this case, the beam passes near through the edge of the lens, i.e., outside the effective diameter. As a result, the beam profile is degraded due to unintentional refraction or some interference. However, when the mirror angle is changed in addition to the lens shift, the beam can be adjusted to pass through and around the lens center as shown in Fig. 8(c). In this case, no degradation in its mode profile is expected.

According to this concept, we demonstrated beam emission angle control of the LISEL. Figure 9(a) shows the photograph of the top view of the fabricated LISEL. The

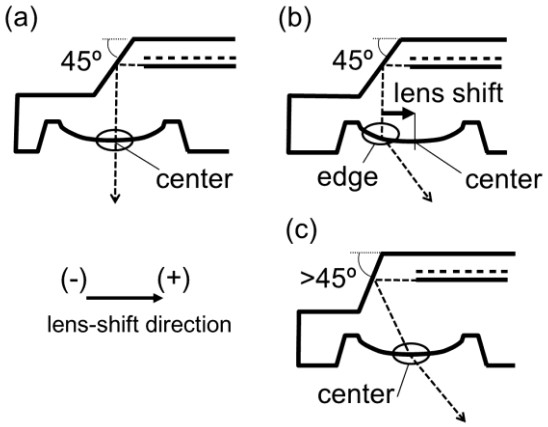

Fig. 8 Principal of emission-beam control. (a) standard position (vertical emission), (b) angled beam with lens shift, and (c) angled beam with lens shift and mirror angle shift from 45°.

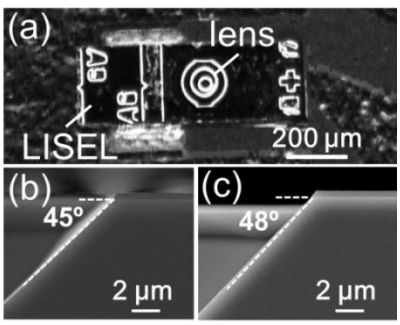

Fig. 9 Fabricated LISEL for SiP platform. (a) Top view of the device with integrated lens, (b) and (C) cross-section of SEM images of 45° and 48° mirror, respectively.

position of the lens is defined by the photo-lithography process, and the R of the lens was chosen to 100 μm for a focused beam to fit the spot of the GC. Cross-sectional SEM images of the mirrors are shown in Fig. 9(b) and (c). Both 45° and 48° mirrors were fabricated to evaluate the beam emission angle with respect to the mirror angle change. Here, measured variation of the mirror angle was 0.5° for 3σ by optimizing the etching process.

Figure 10 shows the emission angle with respect to the lens shift position with the mirror angle from 45° to 48°. Here, the 0 μm of the horizontal axis means that the main beam passes through the center of the lens at each mirror angle (i.e., see Fig. 8(a) for 45° mirror and Fig. 8(c) for mirror angle over 45°). As shown in this graph, a large emission angle of 18.3° was successfully obtained with the mirror angle of 48° and lens shift of -1.0 μm. Moreover, measured emission angles with respect to the lens shift around $+/-5$ μm were in good agreement with the calculated result. Almost the same emission angle of 17.5° was also obtained with the mirror angle of 45°, however, the lens-position shift was large value of 13.5 μm. Measured FFPs of each condition are shown in Fig. 11. V and H direction are parallel and perpendicular to the DFB cavity, respectively. As shown in Fig. 11(a), a large degradation occurred in the case

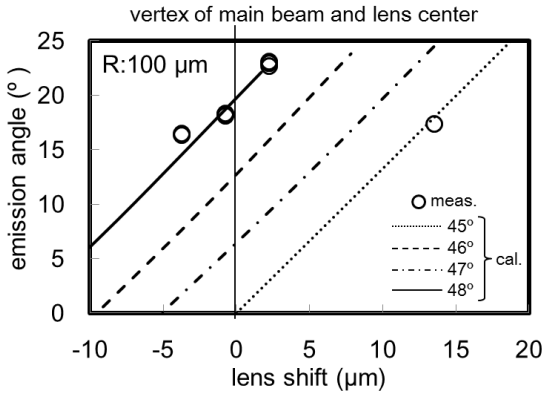

Fig. 10 Emission angle vs lens shift under various mirror angle.

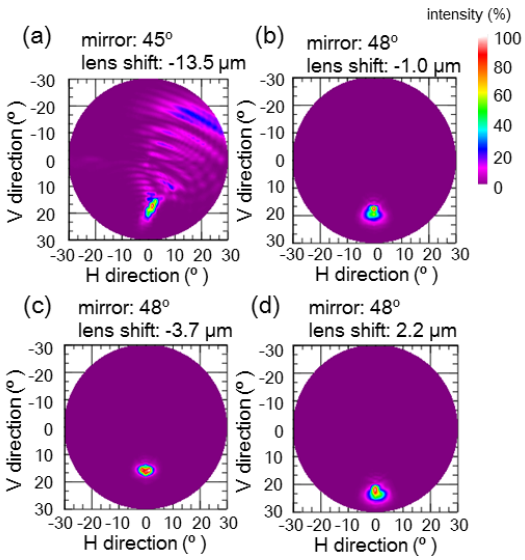

Fig. 11 Measured far-filed patterns, (a) mirror angle of 45°, (b), (c), and (d) mirror angle of 48°.

of 45° mirror. So, it is experimentally observed that a large lens-position shift causes a mode-profile degradation. On the other hand, as shown in Fig. 11(b), (c), and (d), no significant degradation has been observed for the mirror angle of 48°. This indicates that the combination of mirror-angle changing and lens-position shift is an effective way to avoid the degradation of mode profile.

Moreover, from these results, an emission angle up to 20° is thought to be possible without degradation because other mirror angles can be also realized by optimizing fabrication process. These results indicate that the proposed LISEL can provide wide-range emission angle without degradation of its mode profile.

Finally, we demonstrated optical coupling between the LISEL and GC. In this study, two types of LISEL were fabricated to estimate the coupling loss between the LISEL and GC on the SiP platform. One emitted a divergent beam, and the other emitted a focused beam. The mirror angle of the LISEL was 48° in each case. Figure 12 shows the coupling efficiencies as a function of the distance between

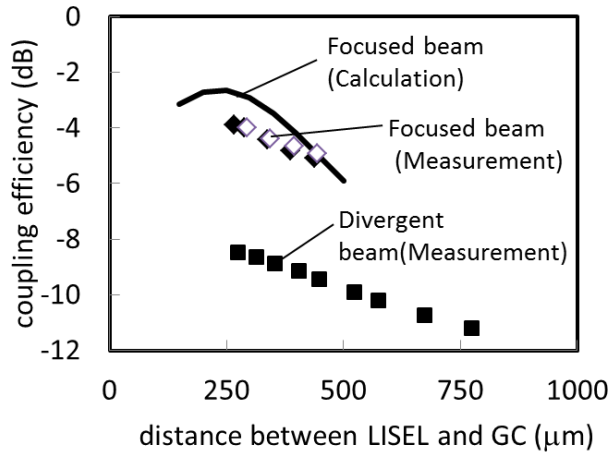

Fig. 12 Coupling loss from LISEL to GC.

the LISEL and GC. In this case, coupling efficiency consists of diffraction efficiency and mode mismatch effect between the LISEL and GC. The incident angle to the GC was set to the diffraction angle of the GC. When the R was large (120 μm), the divergent beam was emitted from the LISEL, and the coupling loss was high (about −8.5 dB) because the mode field of the beam emitted from the LISEL at the GC surface was larger than the size of the GC. In contrast, when the R was small (90 μm), the focused beam was emitted from the LISEL. We evaluated two LISELs with the same design. In each case, a low coupling loss of about −3.9 dB was achieved because the mode field from the LISEL at the GC fitted the size of the GC. Although the beam waist position from the LISEL was about 250 μm, which is shown in the calculation result, the minimum distance to the GC in this experiment was about 270 μm due to limitations in our experimental setup.

This means that if the LISEL could be mounted closer to the GC, the coupling loss could be further reduced. From these experimental results, it was confirmed that the low coupling loss between the LISEL and GC was obtained by the well-controlled R.

4. Facet-Free Structure for Non-Hermetic Package

For cost-effective packaging, a non-hermetic assembly is another key issue to overcome. In terms of the conventional DFB laser, facet coating prevent it from adopting the non-hermetic package [11]. We therefore proposed perfectly facet-free DFB laser based on a LISEL. A distributed Bragg reflector (DBR) mirror and a photodetector (PD) or absorption layer are monolithically integrated at the end of the LISEL, and its rear end is buried with bulk InP (i.e., so-called window structure [18]) as shown in Fig. 13. In this rear-facet free structure, the PD and the window structure can provide the same function as the AR facet coating, which is usually used at the DBR facet to avoid residual reflection [19]. A uniform grating was adopted in the DFB region.

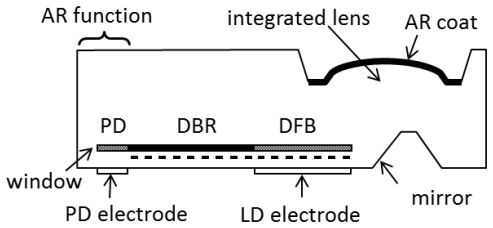

Fig. 13 Schematic structure of facet-free DFB laser based on the LISEL.

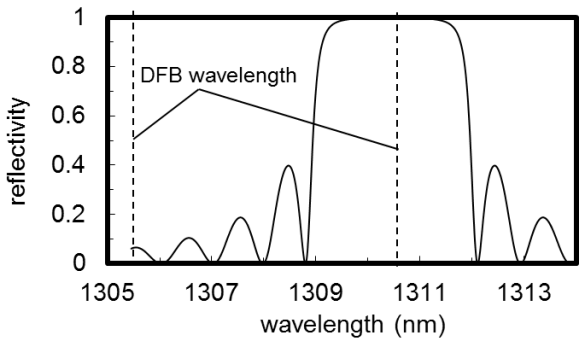

Fig. 14 Theoretical calculation of DBR reflective and two lasing wavelengths of DFB laser with uniform grating.

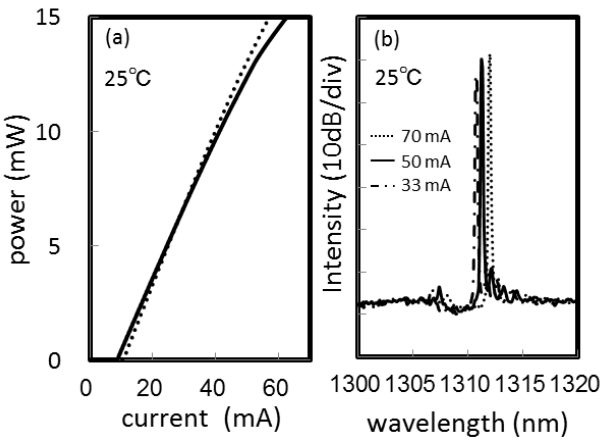

Fig. 15 Lasing characteristics of the DFB laser with facet-free structure, (a) light current curve, and (b) lasing spectra at bias current of 33, 50, 70 mA.

To obtain a stable single-mode operation, DBR and DFB wavelength are needed to be design appropriately. Figure 14 shows the calculated DBR reflection spectrum and wavelength of DFB lasing mode. In this design, one of the two DFB modes is in the stop band of the DBR mirror to obtain a single-mode operation. In this design, one of the two DFB modes is always selected. So we can expect higher single-mode yield as compared to the quarter-ramda shifted grating DFB laser.

Firstly, we evaluated basic lasing characteristics of the DFB laser with the proposed facet-free structure. Figure 15(a) shows the measured light-current characteristic, and the data of the laser with the conventional DBR mirror and AR coating is also plotted. These characteristics are

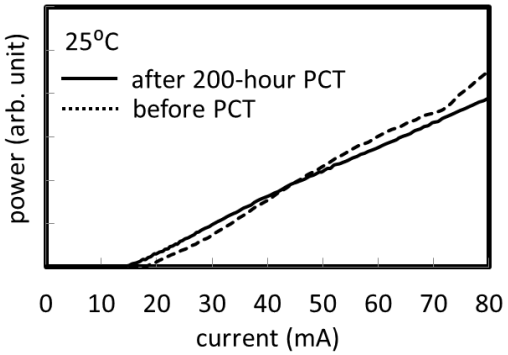

Fig. 16 Measured light-current characteristics of facet-free DFB laer before/after PCT.

almost the same, which indicates the proposed facet-free structure work the same as the conventional DBR and AR coating. Measured lasing spectra are shown in Fig. 15(b). A Stable single-mode operation at high-bias current up to 70 mA was successfully obtained due to the appropriate cavity design.

Next, the facet-free DFB laser was subjected to a 200-hour saturated pressure-cooker test (PCT) at 138°C and 85% RH. Measured light-current characteristics before and after the PCT are shown in Fig. 16. The facet-free DFB laser showed almost the same lasing characteristics with no significant degradation after the 200-hour PCT. These results experimentally confirm for the first time that a laser with a facet-free structure can supply high reliability under high-humidity conditions.

5. Conclusion

A lens-integrated surface-emitting DFB laser (LISEL) and its application to low-cost single-mode OSAs are proposed and discussed. By using LISEL technology, highly-efficient optical coupling with reduced number of optical components and non-hermetic packaging are demonstrated, which enables cost-effective OSAs.

A 4-ch passive alignment optical coupling to an SMF array without an external lens with the coupling efficiency from −3.51 to −2.43 dB has been shown to be achievable by optimizing the integrated lens of the LISEL.

As a light source for SiP, the LISEL μ-platform was proposed, which consists of only a LISEL and a carrier. The emission-beam angle from the LISEL can be controlled by controlling the mirror angle and displacing the lens to fit the diffraction angle of GC. Moreover, by using focused beam, coupling loss between the LISEL and GC was improved to −3.9 dB as compared to using divergent beam of −8.5 dB.

Facet-free structure using LISEL was demonstrated for non-hermetic packaging. The LISEL with a proposed facet-free structure, consisting of a DBR mirror, a PD, and window structure on its end facet, showed the same lasing performance as the conventional laser with AR facet coating. A 200-hour saturated pressure-cooker test (PCT) at 138°C and 85% RH showed no degradation in lasing characteristics. Our results indicate that the LISEL is one of promising light sources for creating cost-effective OSAs.

References

[1] http://www.ieee802.org/3/bs/
[2] http://www.cwdm4-msa.org/
[3] http://www.psm4.org/
[4] K. Adachi, A. Takei, T. Suzuki, S. Tanaka, A. Nakanishi, and K. Naoe, "High-efficiency Optical Coupling to SMF Array and High-temperature 25-Gb/s Operation of Lens-Integrated Surface-Emitting Laser toward PSM4 Optical Module," Proc. European Conference on Optical Communication 2014, Tu.1.1.2, 2014.
[5] A. Narasimha, B. Analui, E. Balmater, A. Clark, T. Gal, D. Guckenberger, S. Gutierrez, M. Harrison, R. Ingram, R. Koumans, D. Kucharski, K. Leap, Y. Liang, A. Mekis, S. Mirsaidi, M. Peterson, T. Pham, T. Pinguet, D. Rines, V. Sadagopan, T.J. Sleboda, D. Song, Y. Wang, B. Welch, J. Witzens, S. Abdalla, S. Gloeckner, and P.D. Dobbelaere, "A 40-Gb/s QSFP Optoelectronic Transceiver in a 0.13 μm CMOS Silicon-on-Insulator Technology," Proc. Optical Fiber Communication Conference 2008, OMK7, 2008.
[6] A.W. Fang, E. Lively, Y.H. Kuo, D. Liang, and J.E. Bowers, "A Distributed Feedback Silicon Evanescent Laser," Opt. Express., vol.16, no.7, pp.4413–4419, 2008.
[7] P.D. Dobbelaere, "External source approach for silicon photonics transceivers," Proc. European Conference on Optical Communication 2014, WS-1, 2014.
[8] B. Pezeshki, J. Heanue, D. Ton, T. Schrans, S. Rangarajan, S. Zou, G.W. Yoffe, A. Liu, M. Sherback, J. Kubicky, and P. Ludwig, "High Perfomance MEMS-Based Micro-Optic Assembly for Mulit-Lane Transceivers," IEEE J. Lightwave technol., vol.32, no.16, pp.2796–2799, 2014.
[9] T. Murao, N. Yasui, K. Mochizuki, M. Shimono, H. Kodera, D. Morita, T. Yamatoya, and H. Aruga, "Lens Alignment Technique Using High-Power Laser for Hybrid Integrated Multi-Channel Transmitter Optical Sub-Assemblies," IEEE Photon. Technol. Lett., vol.25, no.20, pp.1958–1960, 2013.
[10] M. Fukuda, F. Ichikawa, H. Sato, S. Tohno, and T. Sugie, "Pigtail type laser modules entirely moulded in plastic," Electron. Lett., vol.31, no.20, pp.1745–1747, 1995.
[11] N. Chand, J.W. Osenbach, T.L. Evbanosky, R.B. Comizzoli, and W.T. Tsang, "High-Reliability 1.3-μm InP-Based Uncooled Lasers in Nonhermetic Packages" J. Quantum. Electron., vol.32, no.9, pp.1606–1614, 1996.
[12] M. Newkirk, A. Benzoni, J. Paslaski, P. Sercel, C. Tsai, and R. Wyss, "Reliable etched-facet, surface-mount InGaAlAs MQW FP laser at 1.3μm for non-hermetic applications," Proc. The IEEE 24th Annu. Photon. Soc. Meeting, TuD5, 2011.
[13] K. Adachi, K. Shinoda, T. Kitatani, T. Fukamachi, Y. Matsuoka, T. Sugawara, and S. Tsuji, "25-Gb/s Multichannel 1.3-μm Surface-emitting Lens-Integrated DFB Laser Array," IEEE J. Lightwave. Technol., vol.29, no.19, pp.2899–2905, 2011.
[14] T. Suzuki, K. Adachi, A. Takei, K.R. Tamura, A. Nakanishi, K. Naoe, T. Ohtoshi, K. Nakahara, S. Tanaka, and K. Uomi, "Cost-Effective Optical Sub-Assembly Using Lens-Integrated Surface-Emitting Laser," J. Lightwave. Techolo., vol.34, no.2, pp.358–364, 2016.
[15] K. Adachi, K. Shinoda, T. Kitatani, D. Kawamura, T. Sugawara, and S. Tsuji, "40-Gb/s/ch Operation of 1.3-μm Four-wavelength Lens-integrated Surface-emitting DFB Laser Array," Proc. International laser conference, TuB5, 2012.
[16] K. Adachi, A. Takei, T. Suzuki, S. Tanaka, A. Nakanishi, and K. Naoe, "Large-tolerant direct coupling to an SMF array with a lens-integrated suface-emitting laser," IEEE Photon. Technol. Lett., vol.27, no.9, pp.939–942, 2015.
[17] K. Adachi, T. Suzuki, A. Takei, K. Nakahara, S. Tanaka, A.

Nakanishi, and K. Naoe, "Monolithically integrated 4 ch x 25.8 Gbps lens-integrated surface-emitting DFB laser array directly coupled to SMF," IEICE Electron. Express., vol.13, no.12, pp.1–6, 2016.

[18] S. Hirata, K. Tamamura, and C. Kojima, "λ/4-Shifted AlGaAs/GaAs DFB lasers with double window structures," Electron. Lette., vol.23, no.12, pp.627–628, 1987.

[19] M. Matsuda, A. Uetake, T. Simoyama, S. Okumura, K. Takabayashi, M. Ekawa, and T. Yamamoto, "1.3-um-Wavelength AlGaInAs Multiple-Quantum-Well Semi-Insulating Buried-Heterostructure Distributed-Reflector Laser Arrays on Semi-Insulating InP Substrate," IEEE, J. Select. Topic. In Quantum. Electron., vol.21, no.6, 150237, 2015.

Koichiro Adachi received the B.S. and M.S. degrees in physics from Tokyo University of Agriculture and Technology, Tokyo, Japan, in 2003 and 2005, and the Ph.D. degrees in electronics and applied physics from Tokyo Institute of Technology, Tokyo, Japan, in 2016, respectively. In 2005, he was with the Central Research Laboratory, Hitachi, Ltd., where he has been involved in the research and development of photonic devices. He worked on directly-modulated lasers, especially lens-integrated surface-emitting lasers. In 2016, he joined on Oclaro Japan, Inc. and is currently working in technology innovation department.

Takanori Suzuki received the Ph.D. degrees from Keio University, Tokyo, Japan, in 2006. In 2006, he was with the Central Research Laboratory, Hitachi, Ltd., where he has been involved in the research and development of photonic devices. He worked on wavelength-tunable lasers, direct modulated lasers especially lens-integrated surface-emitting lasers and slilicon-photonics switches. In 2016, he joined on Oclaro Japan, Inc. and is currently working in technology innovation department.

Shigehisa Tanaka received the B.S. and M.S. degrees in Electrical Engineering from Kyoto university in 1987 and 1989, respectively. In 1989, he joined the Central Research Laboratory, Hitachi, Ltd., where he has been involved in the research and development of semiconductor materials and photonic devices. Since 2014, he has been the Director of the Technology Innovation Department of Oclaro Japan, Inc.